RESEARCH ARTICLE | APRIL 09 2026

Non-ideal two-dimensional electronic spectroscopy: Theory for a transparent nonlinear system

Special Collection: Computational Spectroscopy

Darius Abramavičius ; Liutauras Pocius

J. Chem. Phys. 164, 144115 (2026)
https://doi.org/10.1063/5.0325578

The Journal of Chemical Physics ARTICLE pubs.aip.org/aip/jcp

Non-ideal two-dimensional electronic spectroscopy: Theory for a transparent nonlinear system

Cite as: J. Chem. Phys. 164, 144115 (2026); doi: 10.1063/5.0325578
Submitted: 31 January 2026 • Accepted: 11 March 2026 •
Published Online: 9 April 2026

Darius Abramavičius[a] and Liutauras Pocius

AFFILIATIONS

Institute of Chemical Physics, Physics Dept., Vilnius University, Saulėtekio al. 3, Vilnius, Lithuania

Note: This paper is part of the Special Topic on Computational Spectroscopy.
[a]**Author to whom correspondence should be addressed:** darius.abramavicius@ff.vu.lt

ABSTRACT

The necessary requirement for an ideal two-dimensional electronic spectroscopy experiment is utilization of ultrashort optical pulses with rectangular spectra for pulse envelopes, while the system transitions fall within the optical pulse window. In this case, the obtained spectra shows clear resonances of the sample response function and various quantum transitions are mapped onto the two-dimensional spectra without distortions. Such conditions, however, are not realistic: first, the pulses never have such spectral profile; second, there may be many transitions that are away from the optical window. In this paper, we present general practical expressions for simulating two-dimensional electronic spectroscopy measurements with specific pulse spectral profiles, and we demonstrate that the off-resonant transitions may have large contributions to the spectra especially at short delay times, when pulse overlaps are significant.

I. INTRODUCTION

Coherent two-dimensional electronic spectroscopy (2DES) over the past 20 years has become a routine spectroscopic tool, which targets ultrafast coherent and relaxation phenomena. In the electronic optical region of visible light from its primary applications,[1,2] the approach was very successful in revealing complex phenomena. Excitonic couplings and ultrafast energy transfer,[3–9] photoinduced charge transfer,[10–13] and coherent electronic and vibrational dynamics[3,14–22] have been revealed in photosynthesis studies. The approach has additionally evolved into more elaborate methods, involving microscopy and nanoscopy, especially using the action detection approach[23–26] as well as extending to even higher orders in the field, which enabled direct observation of multiple excitons and exciton–exciton annihilation processes.[27–30] Possibilities of dissecting charge transfer states have been described by using Stark 2D spectroscopy.[31] Fluorescence excitation spectroscopy has also been extended to two dimensions combining spectral resolution during the excitation process, with exclusive monitoring of the excited-state system dynamics at high time and frequency resolution.[32] Having enormous potential revealing coherent phenomena, two-dimensional spectroscopy has been suggested as a promising tool for quantum technology applications for device studies.[33,34]

Multidimensional spectroscopic techniques have revealed dynamical information about ultrafast electronic energy conversion in technological applications, such as organic solar cells, revealing cooperation between coherent and dissipative phenomena in charge separation,[35,36] as well as synthetic bioinspired systems.[37–39] It has been shown that the vibrational wave-packet is retained from the exciton to the photo-generated hole in the crystalline P3HT domain. Hole delocalization has also been estimated via diminishing of the Huang–Rhys factor via exchange narrowing. Hole transfer dynamics in photovoltaic systems is often characterized with spectrally distant bands. This is targeted by multispectral two-dimensional electronic spectroscopy using both visible and near-IR probes thus considerably extending the probing window.[40,41]

Further on, we consider only the coherent detection regime, which is induced by third-order nonlinear response.[42,43] In most of the applications, the data are usually interpreted by adopting the ideal scenario: the pulses are extremely short, coherent, and

transform-limited, so that pulse overlap effects can be ignored. In this case, the 2DES spectrum directly reflects the specific interaction configurations reflected in the material response function.[43–45]

However, at short delay times, pulse overlaps become important. Certain studies have considered pulse interchange effects. Paleček *et al.* pointed out that the early time dynamics can be dominated by the "incorrect" pulse ordering signals, which affect kinetics at positive times well beyond the pulse overlap region, especially when the "correct" pulse ordering signals are much weaker. Such non-sequential pulse ordering contributions are oscillatory and overlap with the spectral signatures of energy transfer.[46] Pulse overlap effects are especially important in so-called double-quantum coherence spectroscopy, as pointed out by Hedse *et al.*[47] The signal then is short-lived; consequently, a significant part of it is generated during the pulse overlap. It has been shown that the pulse-overlap artifact can be significantly stronger than the required double coherence signal, and only at pulse separations larger than 1.5 times, the pulse length pulse overlap effects are avoided.

In addition, interpretation of the measurement is usually limited to resonant signals. At short delay times, off-resonant optical transitions also contribute, as is often denoted by virtual pathways. Note that for samples with broad absorption bands, the excitation laser spectrum often covers only part of the absorption spectrum, what is especially the case in solar cell or synthetic nanotube studies.[31,35,40,41,48,49] Additional transitions, which are away from the excitation window, may affect the spectra via non-resonant processes in the pulse overlap regions. This becomes an important process when excitations are short lived as is the case in synthetic systems.

In this paper, we derive general expressions for the coherent 2DES signal in the frequency representation, including all field permutations. The expression contain the full response function, where resonant and off-resonant processes can be included. The frequency representation is convenient when considering realistic optical pulse spectra, which can be directly plugged into the obtained expression and then calculations can be performed under realistic experimental conditions using experimental pulse profiles. We demonstrate the power of the approach for extreme cases of "transparent" nonlinear medium due to classical Kerr nonlinearity and demonstrate that under these off-resonant conditions, the 2DES spectrum displays the diagonal peak, which is dynamic due to pulse chirp or due to solvent vibrations.

II. 2DES SIGNAL AMPLITUDE IN THE FREQUENCY DOMAIN

Two-dimensional electronic spectroscopy is realized by using three ultrashort excitation pulses with controlled wave-vectors $\boldsymbol{k}_1$, $\boldsymbol{k}_2$, and $\boldsymbol{k}_3$, while the signal is measured in phase matching wave mixing configurations $\mp\boldsymbol{k}_1 \pm \boldsymbol{k}_2 + \boldsymbol{k}_3$. At low excitation intensity, the major source of the signal is due to the third-order response function. In the simple theoretical scheme, the measurement is performed by a fourth heterodyne pulse, so that the amplitude (not the intensity) of the induced polarization can be recorded.[42,43] As the excitation and detection is impulsive, the delays between pulses become the control parameters. We denote them by T_1, T_2, and T_3. All of them are required to be non-negative (see scheme in Fig. 1). This is achieved by controlling pulse delays in the lab. The

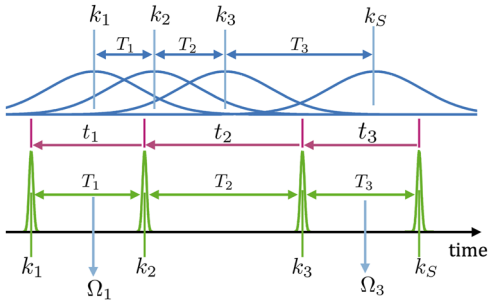

FIG. 1. Scheme of the ideal (green) pulse sequence and the realistic (blue) pulse sequence in 2DES measurement, where delays between interactions t_i and between pulses T_i do not coincide.

two-dimensional spectrum is then obtained by performing signal Fourier transform with respect to delays $T_1 \to \Omega_1$ and $T_3 \to \Omega_3$ scanning both T_1 and T_3 from 0 to infinity. T_2 remains the waiting time parameter, which tracks system evolution, i.e., the correlations between amplitudes in Ω_1 and Ω_3 dimensions.

The 2DES measurement is often associated with system interaction pathways, which are encoded into the third-order response function:[42] $S^{(n)}(t_3,t_2,t_1) = (-i)^3\theta(t_3)\ldots\theta(t_1)\langle\hat{P}\mathcal{G}(t_3)\mathcal{V}\ldots\mathcal{G}(t_1)\mathcal{V}\rho_0\rangle$. Here, $\langle\ldots\rangle$ denotes the trace operation; ρ_0 is the equilibrium density matrix of the system; and $\hat{P}$ is the polarization (or dipole) operator, while $\mathcal{V}\hat{o} = [\hat{P},\hat{o}]$ is the corresponding commutator super-operator for an arbitrary operator $\hat{o}$. Finally, $\mathcal{G}(t)\hat{o} = \exp(-i\hat{H}t)\hat{o}\exp(i\hat{H}t)$ is the propagator (super-operator) for a system described by Hamiltonian $\hat{H}$. In the following, we consider $\hbar = 1$. Heaviside functions $\theta(t)$ are due to causality.

Various interaction configurations take place due to commutators. The interactions are conveniently displayed as Feynman diagrams (see Fig. 2). Under resonance conditions and ignoring pulse overlaps, three Feynman diagrams contribute to $-\boldsymbol{k}_1 + \boldsymbol{k}_2 + \boldsymbol{k}_3$ (rephasing) configuration. These reflect ground state bleaching (GSB), excited state emission (ESE), and excited state absorption (ESA) contributions. Similarly, other three Feynman diagrams contribute to $\boldsymbol{k}_1 - \boldsymbol{k}_2 + \boldsymbol{k}_3$ (non-rephasing) configuration. Two additional diagrams of the third-order response correspond to the double-quantum coherence (2q) signal at $\boldsymbol{k}_1 + \boldsymbol{k}_2 - \boldsymbol{k}_3$ phase matching configuration. The three configurations of the response function show specific phase rotation in the three time delays: rephasing configuration implies $S^{(3)}_{rp}(t_3,t_2,t_1) \sim \exp(i\varepsilon(t_1 - t_3) - i\eta t_2)$, non-rephasing $S^{(3)}_{nr}(t_3,t_2,t_1) \sim \exp(-i\varepsilon(t_1 + t_3) - i\eta t_2)$, while double-quantum coherence $S^{(3)}_{2q}(t_3,t_2,t_1) \sim \exp(-i\varepsilon(t_1 + t_3) - i2\varepsilon t_2)$. Here, ε is the electronic transition frequency resonant to the optical field, while η may reflect slow processes ($\eta \ll \varepsilon$), such as vibrational oscillation or energy relaxation. In the ideal case (see Fig. 1), the 2DES spectrum is directly proportional to these components of the response function. Indeed that becomes possible when pulses are ideally short (see Fig. 1 green pulses) since pulse delays T_i directly correspond to the interaction delays t_i. However, the full response function is a sum of all diagrams with all kinds of phase oscillations and we consider it as such in the following.

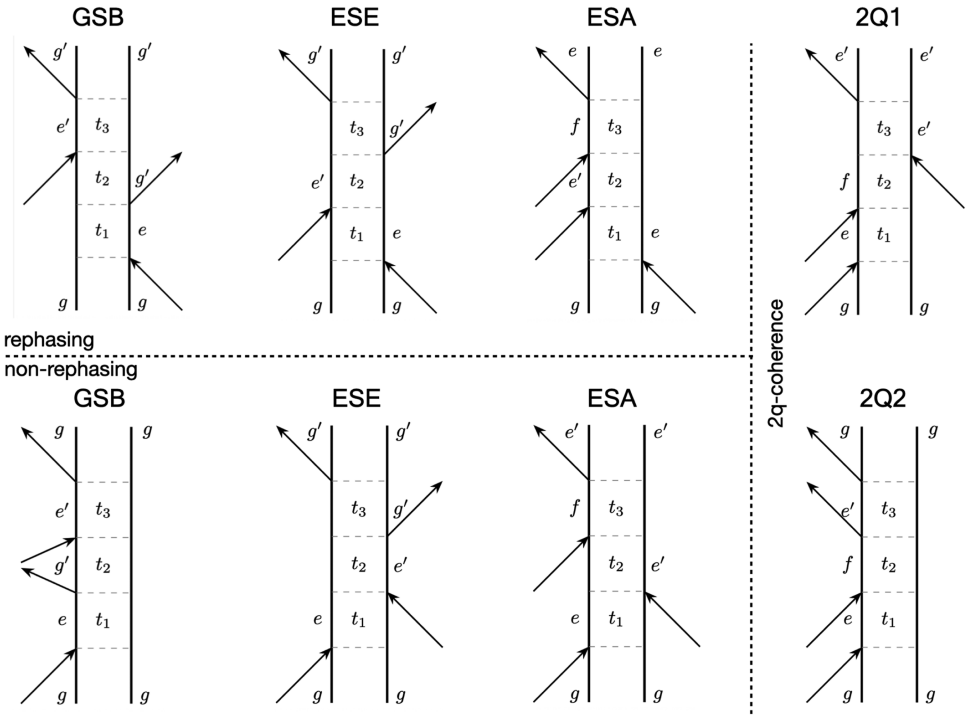

FIG. 2. Feynman diagrams for the third-order response function for the rephasing, non-rephasing, and double-quantum (2q) coherence interaction configurations.

The nonlinear response is much more complicated when the field pulses are not ideal, as represented in Fig. 1 by the blue pulses. In this case, the pulse delays T_i and interaction delays t_i are different and the interaction sequence may be different than the pulse sequence. The explicit pulse envelopes have to be explicitly included in calculations in this case. Nonlinear spectroscopy is induced by a nonlinear medium, which mixes incoming fields and generates the mixed optical response.

A general response function theory is the basis of the formulation of nonlinear optics. The theory connects the total incoming field $E_{tot}(t)$ with the induced third-order nonlinear polarization $P^{(3)}(t)$ via non-local convolution expression, which involves the total nonlinear response function $S^{(3)}$,[42]

$$P^{(3)}(t) = \iiint_0^\infty dt_3 dt_2 dt_1 S^{(3)}(t_3, t_2, t_1) E_{tot}(t - t_3) \times E_{tot}(t - t_3 - t_2) E_{tot}(t - t_3 - t_2 - t_1). \quad (1)$$

In the following, we assume that the response function is known. The expression implies driving the system out of equilibrium by external fields and expressing the expectation value of the non-equilibrium polarization essentially as the source of the new outgoing field. Hence, $E_{out}(t) \sim P(t)$. Note that specific realizations of the measurement may lead to the presence of an overall phase shift;[50] however, this will just give a phase rotation of the result.

Consider the three excitation pulses applied onto the nonlinear sample. For the three pulses, the total optical field is given by their sum,

$$E_{tot}(t) = E_3(t) + E_2(t) + E_1(t) + c.c. \quad (2)$$

Here, each incoming field is characterized by its wave-vector $\boldsymbol{k}_i$ and carrier frequency ω_i, i.e., $E_i(t) = \mathcal{E}_i(t) \exp(i\boldsymbol{k}_i\boldsymbol{r} - i\omega_i t)$; $\mathcal{E}_i(t)$ is the pulse envelope and *c.c.* denotes complex conjugation. The measurement is performed at the mixed wave-vector. Let us focus on the rephasing wave vector configuration,

$$\boldsymbol{k}_{rp} = -\boldsymbol{k}_1 + \boldsymbol{k}_2 + \boldsymbol{k}_3. \quad (3)$$

The total field is taken to third power in Eq. (1), while at various delay times, each $E_{tot}(t - \tau)$ consists of six terms Eq. (2). Then, the following six field multiplication configurations lead to the $\boldsymbol{k}_{rp}$ signal, where we denote

$$\mathcal{F}_{rp}(s_3, s_2, s_1) = E_3(s_3)E_2(s_2)E_1^*(s_1) + E_3(s_3)E_1^*(s_2)E_2(s_1) + E_2(s_3)E_3(s_2)E_1^*(s_1) + E_2(s_3)E_1^*(s_2)E_3(s_1) + E_1^*(s_3)E_3(s_2)E_2(s_1) + E_1^*(s_3)E_2(s_2)E_3(s_1). \quad (4)$$

Here, we used short notation for delays: $s_3 = t - t_3, s_2 = t - t_3 - t_2, s_1 = t - t_3 - t_2 - t_1$. In the heterodyne detection mode, additional fourth pulse $E_4(t)$ is applied for detection purpose as a local heterodyne field along the desired signal wave-vector. Hence, it does not mix in Eq. (1), while it enables the measurement of the induced polarization amplitude. The detected signal is then given by integral,

$$R_{rp} = \int_{-\infty}^{+\infty} dt_4 P_{rp}^{(3)}(t_4) E_4^*(t_4). \quad (5)$$

Combining these definitions, the signal amplitude is given by four-fold time integral,

$$R_{rp} = \iiint dt_4 dt_3 dt_2 dt_1 S^{(3)}(t_3,t_2,t_1) E_4^*(t_4) \times \mathcal{F}_{rp}(t_4-t_3, t_4-t_3-t_2, t_4-t_3-t_2-t_1). \quad (6)$$

Since the absolute time position is not relevant, one integral can be integrated out. Using Fourier representation of the response function $FT\left\{S^{(3)}(t_3,t_2,t_1)\right\} = \bar{S}^{(3)}(\omega_3,\omega_2,\omega_1)$, one then finds a more compact expression for the signal,

$$R_{rp} = \iint \frac{d\omega_1 d\omega_2 d\omega_3}{8\pi^3} \bar{S}^{(3)}(\omega_3,\omega_2,\omega_1) \tilde{E}_4^*(\omega_3) \times \mathcal{F}_{rp}^{(\omega)}(\omega_3-\omega_2, \omega_2-\omega_1, \omega_1). \quad (7)$$

Here, $\bar{S}^{(3)}, \tilde{E}$ are Fourier images, while the frequency domain permutations are as follows:

$$\begin{aligned}\mathcal{F}_{rp}^{(\omega)}(x_3,x_2,x_1) = {} & \tilde{E}_3(x_3)\tilde{E}_2(x_2)\tilde{E}_1^*(-x_1) + \tilde{E}_3(x_3)\tilde{E}_1^*(-x_2) \times \tilde{E}_2(x_1) + \tilde{E}_2(x_3)\tilde{E}_3(x_2)E_1^*(-x_1) \\ & + \tilde{E}_2(x_3)E_1^*(-x_2)\tilde{E}_3(x_1) + \tilde{E}_1^*(-x_3) \times \tilde{E}_3(x_2)\tilde{E}_2(x_1) + \tilde{E}_1^*(-x_3)\tilde{E}_2(x_2)\tilde{E}_3(x_1). \quad (8)\end{aligned}$$

Notice that instead of four-dimensional time integral, we have a three-dimensional frequency integral. This amplitude explicitly corresponds to the rephasing type measurement. Other measurements expressions are given in Appendix A.

Instead of using full-field Fourier transforms, it is convenient to separate the transforms of the pulse envelope functions, as shown in Appendix B. Fourier transform of a simple pulse may be written as

$$\tilde{E}_i(\omega) = e^{i\boldsymbol{k}_i\boldsymbol{r}+i\omega\tau}\mathcal{E}_i(\omega-\omega_0) + e^{-i\boldsymbol{k}_i\boldsymbol{r}+i\omega\tau}\mathcal{E}_i^*(-\omega-\omega_0), \quad (9)$$

where τ is the pulse reference time (peak position) and ω_0 is its carrier frequency. The envelope spectrum function $\mathcal{E}_i(\omega)$ is assumed to be peaked around zero frequency.

Due to time translational symmetry, the absolute moments of different pulses are not important—only relative positions matter. To apply this expression for 2DES, the absolute time reference is chosen, such that the time of the local oscillator (or detector) $\tau_4 = 0$. The delays between nearby pulses are then defined: $T_1 = \tau_2 - \tau_1$, $T_2 = \tau_3 - \tau_2$, and $T_3 = \tau_4 - \tau_3$. Using these definitions, we write the detected amplitude as the function of the delay times and write it explicitly in terms of pulse spectral envelopes,

$$\begin{aligned}R_{rp}(T_3,T_2,T_1) = {} & \iiint_{-\infty}^{\infty} \frac{d\omega_1 d\omega_2 d\omega_3}{8\pi^3} S^{(3)}(\omega_3,\omega_2,\omega_1)\mathcal{E}_4^*(\omega_3-\omega_0) \times e^{-i\omega_3 T_3}\Big[e^{-i\omega_2 T_2 - i\omega_1 T_1}\mathcal{E}_3(\omega_3-\omega_2-\omega_0) \\ & \mathcal{E}_2(\omega_2-\omega_1-\omega_0)\mathcal{E}_1^*(-\omega_1-\omega_0) + e^{-i\omega_2 T_2 - i(\omega_2-\omega_1)T_1}\mathcal{E}_3(\omega_3-\omega_2-\omega_0) \times \mathcal{E}_1^*(-\omega_2+\omega_1-\omega_0)\mathcal{E}_2(\omega_1-\omega_0) \\ & + e^{-i(\omega_3-\omega_2+\omega_1)T_2 - i\omega_1 T_1}\mathcal{E}_2(\omega_3-\omega_2-\omega_0) \times \mathcal{E}_3(\omega_2-\omega_1-\omega_0)\mathcal{E}_1^*(-\omega_1-\omega_0) \\ & + e^{-i(\omega_3-\omega_1)T_2 - i(\omega_2-\omega_1)T_1}\mathcal{E}_2(\omega_3-\omega_2-\omega_0) \times \mathcal{E}_3(\omega_2-\omega_1-\omega_0)\mathcal{E}_1^*(-\omega_1-\omega_0) \\ & + e^{-i(\omega_3-\omega_2+\omega_1)T_2 - i(\omega_3-\omega_2)T_1}\mathcal{E}_1^*(-\omega_3+\omega_2-\omega_0)\mathcal{E}_3(\omega_2-\omega_1-\omega_0)\mathcal{E}_2(\omega_1-\omega_0) \\ & + e^{-i(\omega_3-\omega_1)T_2 - i(\omega_3-\omega_2)T_1}\mathcal{E}_1^*(-\omega_3+\omega_2-\omega_0) \times \mathcal{E}_2(\omega_2-\omega_1-\omega_0)\mathcal{E}_3(\omega_1-\omega_0)\Big]. \quad (10)\end{aligned}$$

The first term in the expression directly corresponds to the case when pulse ordering coincides with the interaction ordering. Other terms corresponds to various permutations of interaction times. This is implied by the following integration variables: ω_1 is for the first interaction, ω_2 for the second interaction, ω_3–the third interaction, and ω_4–for the detection, while the experiment always maintains $\tau_1 \le \tau_2 \le \tau_3 \le \tau_4$ so $T_1, T_2, T_3 \ge 0$. This form of the integral is demonstrated by the schemes shown in Fig. 3. Here, terms 1–6 in the integral in Eq. (10) correspond to Figs. 3(a)–3(f) correspondingly. Similar expression can also be obtained for $\boldsymbol{k}_{nr} = +\boldsymbol{k}_1 - \boldsymbol{k}_2 + \boldsymbol{k}_3$ and $\boldsymbol{k}_{2Q} = \boldsymbol{k}_1 + \boldsymbol{k}_2 - \boldsymbol{k}_3$ detection configurations, as shown in Appendix A.

The above-mentioned integral emphasizes permutation of excitation pulses. The expression implies infinite frequency integration, while only specific spectral regions defined by pulse spectral profiles are important for different terms. By changing integration variables, we can write a different form, where all pulses have the same integration variables,

$$\begin{aligned}R_{rp}(T_3,T_2,T_1) = {} & \iiint_{-\infty}^{\infty} \frac{dx_1 dx_2 dx_3}{8\pi^3} \mathcal{E}_4^*(x_3)\mathcal{E}_3(x_3-x_2) \times \mathcal{E}_2(x_2-x_1)\mathcal{E}_1^*(-x_1)\exp\left(-i(x_3+\omega_0)T_3 - ix_2T_2 - i(x_1-\omega_0)T_1\right)\Big[S_{4321}^{(3)}(x_3+\omega_0,x_2,x_1 \\ & -\omega_0) + S_{4231}^{(3)}(x_3+\omega_0,x_3-x_2+x_1,x_1-\omega_0) + S_{4312}^{(3)}(x_3+\omega_0,x_2,x_2-x_1+\omega_0) \\ & + S_{4213}^{(3)}(x_3+\omega_0,x_3-x_2+x_1,x_3-x_2+\omega_0) + S_{4132}^{(3)}(x_3+\omega_0,x_3-x_1+2\omega_0,x_2-x_1+\omega_0) \\ & + S_{4123}^{(3)}(x_3+\omega_0,x_3-x_1+2\omega_0,x_3-x_2+\omega_0)\Big]. \quad (11)\end{aligned}$$

The response function now gets different frequency permutations. The subscripts in the response function list the interaction sequence, which is important when considering different pulse polarizations. Hence, $S_{ijkl}^{(3)}$ denotes that the first interaction happens with l pulse, the second with k, third with j, while i is for the signal detection. All integrations are now performed in the vicinity around zero as required by envelopes, while the six configurations of the response functions nicely select resonances. Assuming close to resonant conditions, the terms $S_{4321}^{(3)}(\ldots) + S_{4231}^{(3)}(\ldots)$ can be associated with the rephasing frequency signature. These two terms will be dominant in the rephasing signal expression in the resonance measurement, while the two terms are only due to pulse overlaps. For the remaining terms, $S_{4312}^{(3)}(\ldots) + S_{4213}^{(3)}(\ldots)$ correspond to non-rephasing terms, while $S_{4132}^{(3)}(\ldots) + S_{4123}^{(3)}(\ldots)$ reflects contribution from double-quantum resonances due to $2\omega_0$; as was described

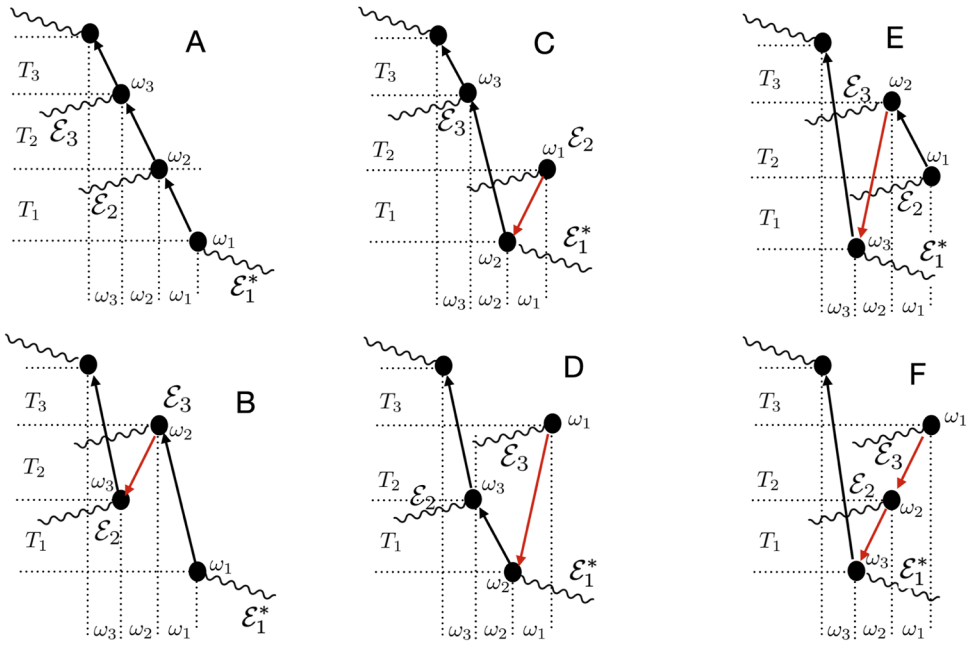

FIG. 3. Scheme of various pulse configurations in 2DES measurement.

above, they are off-resonant in the measurement, but if there are no specific system resonances of the response function to be captured by optical frequency ω_0, the full response function with all response function configurations has to be included in calculating the signal intensity.

Finally, the 2D Fourier transform for positive delay times yields the 2D spectrum $(\Omega_3,\ \Omega_1)$ as a function of the delay time T_2,

$$R(\Omega_3, T_2, \Omega_1) = \iint_0^\infty dT_1 dT_3 e^{i\Omega_3 T_3 + i\Omega_1 T_1} R(T_3, T_2, T_1). \quad (12)$$

Exponent $\exp\left(-i(x_3+\omega_0)T_3 - ix_2T_2 - i(x_1-\omega_0)T_1\right)$ then directly turns into a Lorentzian function. While this can be written explicitly, the frequency integration of Lorentzian functions is slowly converging, so it is more convenient to maintain expressions as functions of time and use numerical fast Fourier transforms instead. Still, the final integration over x–es needs to be performed using specific pulse envelopes.

III. APPLICATIONS

A. Rephasing signal for nonlinear transparent medium

The above-mentioned expression of the 2DES allows calculating the spectrum for an arbitrary response function. Resonant conditions are usually implied. In contrast to this, we consider the transparent nonlinear material (e.g., solvent or protein contributions to the signal), whose fundamental excitation resonances lie, e.g., in deep UV. As a simple nonlinear model, we consider the case of modulation of the index of refraction by the intensity of the optical field, which is known by the Kerr effect.[51] It is described by dependence of the refraction index on the optical field intensity,

$$\Delta n \sim \chi^{(3)} |E_\omega|^2, \quad (13)$$

where $\chi^{(3)}$ is a constant and E_ω is the amplitude at the given frequency ω. Since all electronic transitions are assumed to be off-resonant, the frequency domain response function $S^{(3)}(\omega_3\omega_2\omega_1)$ varies slowly within the pulse envelope spectrum and we can simply put it to a constant, $S^{(3)}(\omega_3\omega_2\omega_1) \approx S_0^{(3)}$. This condition can be understood as related to a very short lifetime of some excited system resonances. Then, the time domain representation response function is essentially given by Dirac deltas,

$$\begin{aligned} S^{(3)}(t_3,t_2,t_1) &= \iiint_{-\infty}^{\infty} \frac{d\omega_1 d\omega_2 d\omega_3}{8\pi^3} e^{-i\omega_3 t_3 - i\omega_2 t_2 - i\omega_1 t_1} S_0^{(3)} \\ &= S_0^{(3)} \delta(t_3)\delta(t_2)\delta(t_1). \end{aligned} \quad (14)$$

Hence, the result implies that the response function decays much faster than the optical pulse length. Then, for all Feynman diagrams, which at specific time interval involves electronic excited states the condition of $S^{(3)}(\ldots, t_i, \ldots) \sim \delta(t_i)$ perfectly applies.

In that case, the signal integrates the optical pulses as determined by Eq. (11). Assuming the Gaussian pulse envelope functions as defined in Appendix B, the signal expression turns to be very simple. We can then write

$$\begin{aligned} R_{rp}(T_3,T_2,T_1) = \frac{3S_0^{(3)}}{4\pi^3} \iiint_{-\infty}^{\infty} dx_1 dx_2 dx_3 g_\sigma(x_3,x_2,x_1) \\ \times \exp\left(-i(x_3+\omega_0)T_3 - ix_2T_2 - i(x_1-\omega_0)T_1\right), \end{aligned} \quad (15)$$

where ω_0 is the pulse carrier frequency,

$$g_\sigma(x_3,x_2,x_1) = \exp\left(-\frac{x_3^2}{\sigma^2} - \frac{(x_3-x_2)^2}{\sigma^2} - \frac{(x_2-x_1)^2}{\sigma^2} - \frac{x_1^2}{\sigma^2}\right), \quad (16)$$

while σ is the pulse bandwidth. We obtain a three-dimensional Gaussian integral, which can be calculated analytically (see Appendix C), leading to time domain signal,

$$R_{rp}(T_3,T_2,T_1) = \frac{3S_0^{(3)}\sigma^3}{8\pi^{3/2}} \exp\left(i\omega_0(T_1-T_3)\right) \exp\left(-\frac{\sigma^2}{16}\left(3T_1^2 + 4T_2(T_2+T_3) + 3T_3^2 + 2T_1(2T_2+T_3)\right)\right). \quad (17)$$

The remaining Fourier transforms for 2D spectra can be performed using FFT algorithms after scanning delay times T_1 and T_3.

It is possible to calculate the signal for the chirped pulses (see Appendix B), however, the quadratic form contains complex values. Instead of full integration, we perform partial integration over x_1 and x_3. This yields a slightly more complicated expression,

$$R_{rp}(T_3,T_2,T_1) = \frac{3S_0^{(3)}\sigma^3 e^{-i\omega_0(T_3-T_1)}}{8\pi^2} \int_{-\infty}^{\infty} dx \exp\left(-\frac{2x^2}{1-i\xi} - ix\sigma T_2\right) \times \exp\left(f(x,\sigma T_1) + f(x,\sigma T_3)\right), \quad (18)$$

where ξ is a dimensionless chirp parameter (Appendix B). In addition, we introduced an auxiliary function,

$$f(x,y) = \frac{1}{8}\left(\frac{2x}{1-i\xi} - iy\right)^2. \quad (19)$$

Notice that only one parameter affects the shape of the signal in this expression: the factor $3S_0^{(3)}\sigma^3/(8\pi^{3/2})$ is just the amplitude scaling parameter and the central frequency ω_0 defines the "window" position, while σ defines the window size and the overall decay time. Thus, the key parameter is ξ, which determines the chirp of the pulse.

Such a case is presented in Fig. 4, where rephasing configuration is used for the 2D spectrum, which is obtained using Gaussian pulses [Eqs. (17) and (18)]. First of all, consider the pure transform-limited Gaussian pulses [no chirp, Fig. 4(a)]. The obtained 2D spectrum reflects the characteristic elongated line shape and orientation, corresponding to the rephasing signal. Notice that this shape is purely related to the field multiplication and does not contain system information apart from the signal amplitude. The peak width is defined by Gaussian envelopes of excitation and detection fields. For simple Gaussian pulses, there is very simple shape-wise dependence on the delay time T_2: the peak decays as a Gaussian and a slight broadening can be observed. The signal thus is important only at short delay times.

Next, we consider the Gaussian chirped pulses. In this case, the spectrum in Fig. 4(b) shows slight dependence on time T_2. The most interesting property is that now there is a phase rotation of the peak with T_2 delay time. Notice that for the linear chirp, as considered in the present case, the effective frequency of the pulse changes within Gaussian envelope linearly as $\omega(t) = \omega_0 + \xi\sigma^2 t$, so within the pulse duration at σ^{-1}, the frequency shift is $\xi\sigma$. Then, the phase rotation occurs with the waiting time T_2 roughly as $\cos(\xi\sigma T_2)$, and thus, it becomes more severe with increasing chirp. Hence, this could be used, e.g., to estimate the pulse chirp.

B. Partially off-resonant system: Including the Raman process

An extension of the above-described off-resonant nonlinear Kerr process includes partially resonant case. Notice that if the transparent medium is a molecular solvent (for example, water), its absorption spectrum is in UV, while molecules of the solvent contain vibrational modes, which cover a 10–3000 cm^{-1} range in the electronic ground state. Such characteristics are inherent for the most widely used solvent, e.g., water. Water vibrations are well-resolved in the time-resolved optical Kerr effect spectroscopy (see, e.g., Ref. 52) as well as in IR and Raman measurements (see, e.g., Ref. 53, while there are many studies). Vibrational excitations decay

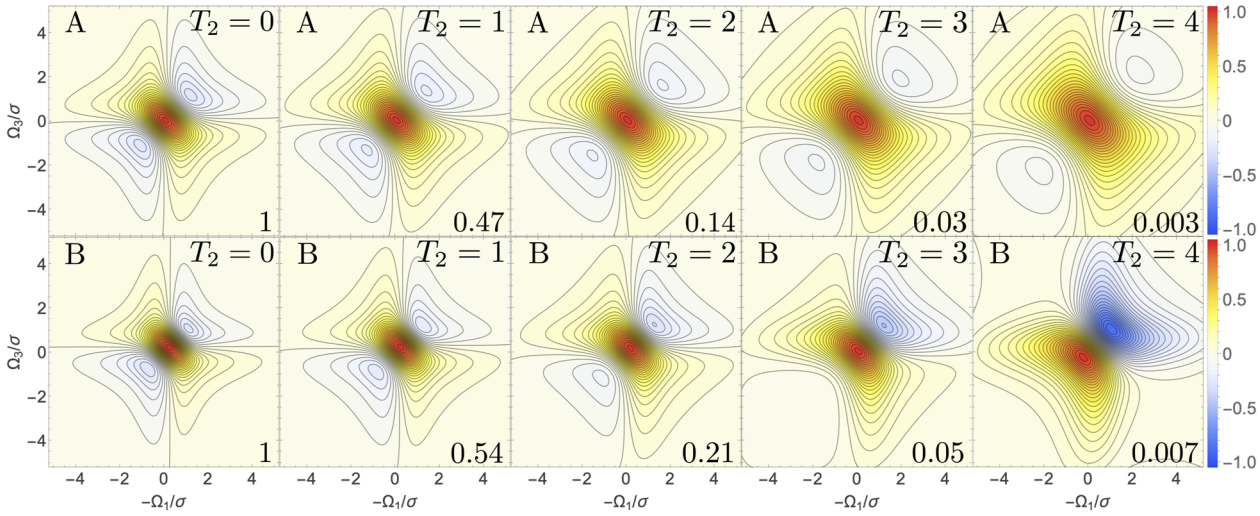

FIG. 4. Simulation of the 2DES rephasing signal for a transparent nonlinear medium using Gaussian pulses. The spectrum is centered at the pulse carrier frequency ω_0. A. Zero chirp, B. Chirped pulse ($\xi = 1$). Amplitude of the spectrum with respect to time $T_2 = 0$ is shown in the insets.

within picoseconds and may strongly affect the optical response function. There are two Feynman diagrams, which directly expose ground state vibrations: GSB of rephasing and of non-rephasing configurations—see Fig. 2, where during the second time interval t_2, the system is in the electronic ground state. In this interval, vibrational states of water molecules may be excited as is the source of the well-known Raman scattering. The rephasing diagram will have phase rotation $\exp(ivt_2)$, where v is the specific vibrational frequency, while non-rephasing diagram will be proportional to $\exp(-ivt_2)$. Vibrations do take place for all other diagrams and in other intervals; however, the system is then in the excited state, which is assumed short-lived, so the response function for other time intervals is still $\sim \delta(t_1)\delta(t_3)$. The combined response function will contain the sum of the two Raman processes and, therefore, be of the form

$$S^{(3)}(t_3, t_2, t_1) \sim \delta(t_1)\delta(t_3)\exp(-\gamma t_2)\cos(vt_2). \tag{20}$$

Here, γ is the vibrational coherence decay rate, which usually corresponds to few picosecond decay time. This response function should be substituted into Eq. (11) and requires the corresponding Fourier image,

$$S^{(3)}(\omega_3, \omega_2, \omega_1) = S_0^{(3)} i\gamma \frac{\omega_2 + i\gamma}{(\omega_2 + i\gamma)^2 - v^2}. \tag{21}$$

Such form guarantees that if $\gamma \to \infty$, $S^{(3)}(\omega_3, \omega_2, \omega_1) \to S_0^{(3)}$, as used in Sec. III A (notice that the time domain response function is a real function, while the frequency domain function is complex). Substituting this function into Eq. (11) and separating the ω_2 integral in all terms, we find only two different terms [the third one is also nonzero, but is $\gamma/(2\omega_0)$ smaller compared to the two which are contained], as shown in Appendix D. The response expression for the chirped Gaussian pulse is thus

$$\begin{aligned} R_I(T_3, T_2, T_1) = {} & \frac{i\gamma\sigma^3 e^{-i\omega_0(T_3 - T_1)}}{8\pi^2} \\ & \times \int_{-\infty}^{\infty} dx \frac{(\sigma x + i\gamma)\exp\left(-ix\sigma T_2 - 2x^2\right)}{(\sigma x + i\gamma)^2 - v^2} \\ & \times \left[\exp\left(f(x, \sigma T_1) + f(x, \sigma T_3) - 2ix^2\xi\right)\right. \\ & + \left.\exp\left(f^*(x, \sigma T_2 + \sigma T_1) + f(x, \sigma T_3 + \sigma T_2)\right)\right]. \end{aligned} \tag{22}$$

Figure 5 presents the calculated 2D spectra of such transparent nonlinear material by including one vibrational mode via the Raman scattering process. Here, we assume a vibrational frequency $v = 500$ cm^{-1} and its decay rate $\gamma = 3$ cm^{-1}. These are relevant parameters for collective C=C bond vibrations and its decay time of 1 ps. The σ value is taken 300 cm^{-1}. The pulse time $\sim \sigma^{-1}$ is of the same order as the vibrational oscillation period so the vibrational oscillation can still be probed along T_2 delay. So, while the electronic resonances are assumed in deep UV, the vibrational beatings of the Raman mode can be clearly observed in 2D spectra as a function of delay time T_2 for zero chirp pulses. The phase rotation is symmetric with respect to the point $\Omega_1 = \Omega_3 = 0$. This is the consequence of the fact that rephasing and non-rephasing response functions contribute equally due to ultrafast decay time during T_1 and T_3 times. Different from Fig. 4, the spectrum amplitude does not decay as a Gaussian: there is a fast component from $T_2 = 0$ to $T_2 = 1$; however, then the spectrum stops decaying and shows only phase rotation as is the case for the resonant ground state vibrations. Figure 5(b) demonstrates the case with nonzero chirp. Similar to Fig. 4(b), there is additional phase rotation due to variation of carrier frequency, which complicates the whole picture even more.

IV. DISCUSSION AND CONCLUSIONS

Ideal measurement of 2DES spectra requires mutually exclusive conditions. Perfect selection of resonances requires pulse spectral

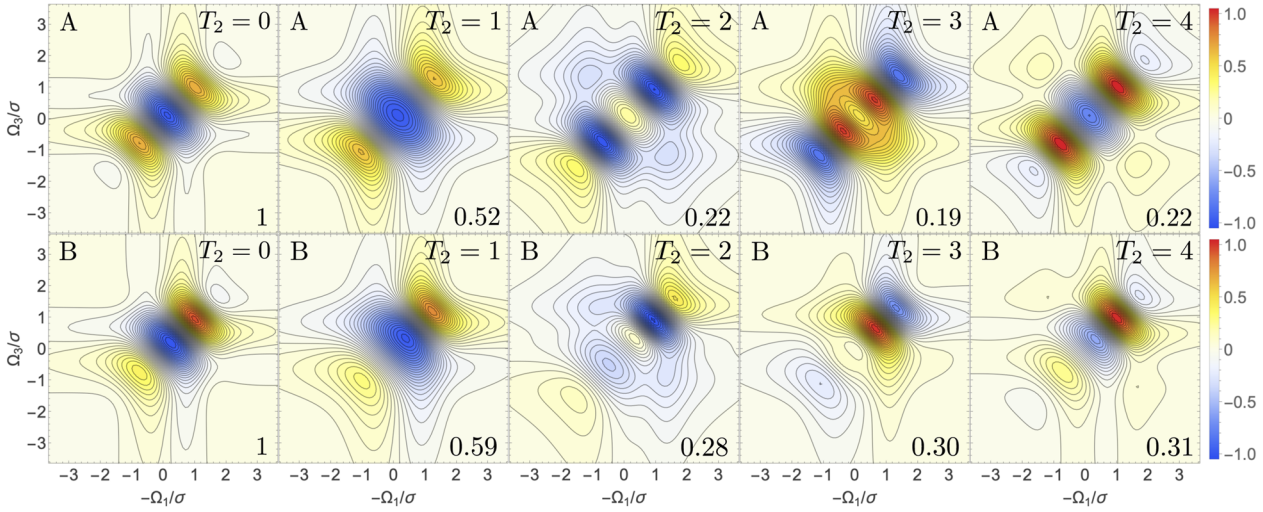

FIG. 5. Simulation of the 2DES rephasing signal for a transparent nonlinear medium, including the Raman process using Gaussian pulses. The spectrum is centered at the pulse carrier frequency ω_0. A. Zero chirp, B. Chirped pulse $\xi = 1/4$. Amplitude of the spectrum with respect to time $T_2 = 0$ is shown in the insets.

widths being much larger than material absorption bandwidths ($\sigma \gg \gamma$ in our notation). While this is roughly satisfied in spectroscopy of photosynthetic complexes, the spectral bands of organic polymers are often highly inhomogeneous and we may often find that pulses do not cover the whole absorption bands. This is even more expressed for ESA contributions, where ESA bands are usually much broader than the linear absorption. In this case, optical coherences decay with the same time as the pulse duration and pulse overlaps dominate. Clear separation of contributions of different Feynman diagrams becomes problematic, as demonstrated for double-quantum signals in Ref. 47.

We additionally point out that under the pulse overlap conditions, the off-resonant optical transitions will also have a significant contribution to the signals. As a result, the notation of "background free" measurement becomes baseless as the various properties of seemingly transparent solvent will be mapped onto the 2D spectra. The complete off-resonant Kerr-type nonlinearity leads to a static background at short delay times, while Raman vibrational transitions of the solvent molecules will map these vibrations onto 2D spectra as T_2−dependent spectral beatings, which persist for long delay times.

Completely off-resonant Kerr effect may hardly be realistic since all solvents or solid matrix materials essentially display some vibrational bands. Solid amorphous matrices may have ultra-wide phonon bands without clear phonon resonances. In this case, the phonon excitations will be also short-lived so Raman resonances may be observable without sharp resonances.[54] Molecular solvents certainly demonstrate vibrational Raman active modes. The corresponding 2DES spectral beatings corresponding to a solvent should be taken into account when considering ultra-sensitive 2DES beating interpretation.[19] There is an open question regarding the intensity of such off-resonant contributions compared to the contributions of the intended system of interest. Overall, the peak intensity scales as transition dipole fourth power and thus roughly follows the absorption square rule. Thus, focusing on the absorption background may give a clue regarding the background of 2DES measurement. However, that question is outside the focus of this paper.

Polarization of the fields may cause additional complexity in integrations of Eqs. (10) and (11). Pulse polarizations have been subject of experiments in photosynthetic aggregates, where specific orientations of pigment molecules in photosynthetic aggregates cause unique amplitudes at various excitation polarization.[19,21,55] Pulse polarizations are controlled in the lab frame, while interaction patterns of the response function (all Feynman diagrams in Fig. 2) get shuffled in Eq. (10) and the full set of tensor components of the response function may be necessary to include. In the dipole approximation, the isotropic sample is characterized by three unique tensor components: *xxyy*, *xyxy*, and *xyyx*, with $S^{(3)}_{xxxx} = S^{(3)}_{xxyy} + S^{(3)}_{xyyx} + S^{(3)}_{xyxy}$, when pulse propagation direction is z.[22,56] This holds for all Feynman diagrams. Equation (10) involves explicitly written pulse permutations so specific tensor components of the response function, which are involved in these different terms can be explicitly assigned. For this reason, in Eq. (11), we label interaction configurations in the response functions as subscripts. Only if measurement is with all parallel polarizations, all response function components will correspond to *xxxx* configurations and the response function can be considered as scalar.

Additional technical element, which has a considerable effect related to interpretations is the chirp of the optical pulses. As we demonstrate, the chirp additionally induces peaks beatings in 2D spectra even without material resonances. Its effect, in principle, is similar to the vibrational beatings, which are observed in molecular systems. While this effect might be sorted out by considering various additional properties (such as relating corresponding beating peaks above or below diagonal line, considering beating phases[19,20,57,58]), confident resonance assignment requires considerable data analysis. Realistic pulses with nonsymmetric spectral profiles may induce additional artifacts, which can be sorted out only after complete response calculation, involving triple integration over excitation and detection pulse spectral profiles.

ACKNOWLEDGMENTS

This research was carried out in the framework of the "Universities' Excellence Initiative" program by the Ministry of Education, Science, and Sports of the Republic of Lithuania under the agreement with the Research Council of Lithuania (Project No. S-A-UEI-23-6) and was funded by the Research Council of Lithuania (Grant No. S-MIP-23-48). Computations were performed on resources at the High Performance Computing Center, HPC Saulėtekis, of the Faculty of Physics, Vilnius University.

AUTHOR DECLARATIONS

Conflict of Interest

The authors have no conflicts to disclose.

Author Contributions

Darius Abramavičius: Conceptualization (lead); Formal analysis (lead); Funding acquisition (lead); Investigation (lead); Methodology (lead); Project administration (lead); Resources (equal); Software (supporting); Supervision (lead); Validation (equal); Visualization (supporting); Writing – original draft (lead); Writing – review & editing (lead). **Liutauras Pocius**: Resources (equal); Software (lead); Validation (equal); Visualization (lead).

DATA AVAILABILITY

The data that support the findings of this study are available from the corresponding author upon reasonable request.

APPENDIX A: EXPRESSIONS FOR NON-REPHASING AND DOUBLE-QUANTUM COHERENCE MEASUREMENTS

For the non-rephasing or double-quantum coherence, $\boldsymbol{k}_{nr} = +\boldsymbol{k}_1 - \boldsymbol{k}_2 + \boldsymbol{k}_3$ and $\boldsymbol{k}_{2q} = \boldsymbol{k}_1 + \boldsymbol{k}_2 - \boldsymbol{k}_3$ detection configurations, the following field permutations become important:

$$\begin{aligned}\boldsymbol{k}_{nr} : & E_3(s_3)E_2^*(s_2)E_1(s_1) + E_3(s_3)E_1(s_2)E_2^*(s_1) \\ & + E_2^*(s_3)E_3(s_2)E_1(s_1) + E_2^*(s_3)E_1(s_2)E_3(s_1) \\ & + E_1(s_3)E_3(s_2)E_2^*(s_1) + E_1(s_3)E_2^*(s_2)E_3(s_1), \qquad \text{(A1)}\end{aligned}$$

$$\begin{aligned}\boldsymbol{k}_{2q}: & E_3^*(s_3)E_2(s_2)E_1(s_1) + E_3^*(s_3)E_1(s_2)E_2(s_1)\\ & + E_2(s_3)E_3^*(s_2)E_1(s_1) + E_2(s_3)E_1(s_2)E_3^*(s_1)\\ & + E_1(s_3)E_3^*(s_2)E_2(s_1) + E_1(s_3)E_2(s_2)E_3^*(s_1); \qquad \text{(A2)}\end{aligned}$$

here again, we use shorthand-notation $s_3 = t - t_3, s_2 = t - t_3 - t_2, s_1 = t - t_3 - t_2 - t_1$. Substituting Fourier transforms of all optical pulses and using time delays, $T_1 = \tau_2 - \tau_1$, $T_2 = \tau_3 - \tau_2$, and $T_3 = 0 - \tau_3$, or $\tau_1 = -(T_3 + T_2 + T_1)$, $\tau_2 = -(T_3 + T_2)$, and $\tau_3 = -T_3$, the non-rephasing and the double-quantum coherence signals are given by

$$\begin{aligned}R_{nr}(T_3,T_2,T_1) = \iiint & \frac{d\omega_1 d\omega_2 d\omega_3}{8\pi^3} S^{(3)}(\omega_3,\omega_2,\omega_1)\\ & \times \mathcal{E}_4^*(\omega_3-\omega_0)e^{-i\omega_3 T_3}\left[e^{-i\omega_2 T_2 - i\omega_1 T_1}\mathcal{E}_3(\omega_3-\omega_2-\omega_0)\right.\\ & \times \mathcal{E}_2^*(-\omega_2+\omega_1-\omega_0)\mathcal{E}_1(\omega_1-\omega_0) + e^{-i\omega_2 T_2 - i(\omega_2-\omega_1)T_1}\\ & \times \mathcal{E}_3(\omega_3-\omega_2-\omega_0)\mathcal{E}_1(\omega_2-\omega_1-\omega_0)\mathcal{E}_2^*(-\omega_1-\omega_0)\\ & + e^{-i(\omega_3-\omega_2+\omega_1)T_2 - i\omega_1 T_1}\mathcal{E}_2^*(-\omega_3+\omega_2-\omega_0)\\ & \times \mathcal{E}_3(\omega_2-\omega_1-\omega_0)\mathcal{E}_1(\omega_1-\omega_0)\\ & + e^{-i(\omega_3-\omega_1)T_2 - i(\omega_2-\omega_1)T_1}\mathcal{E}_2^*(-\omega_3+\omega_2-\omega_0)\\ & \times \mathcal{E}_1(\omega_2-\omega_1-\omega_0)\mathcal{E}_3(\omega_1-\omega_0)\\ & + e^{-i(\omega_3-\omega_2+\omega_1)T_2 - i(\omega_3-\omega_2)T_1}\mathcal{E}_1(\omega_3-\omega_2-\omega_0)\\ & \times \mathcal{E}_3(\omega_2-\omega_1-\omega_0)\mathcal{E}_2^*(-\omega_1-\omega_0)\\ & + e^{-i(\omega_3-\omega_1)T_2 - i(\omega_3-\omega_2)T_1}\mathcal{E}_1(\omega_3-\omega_2-\omega_0)\\ & \times \left.\mathcal{E}_2^*(-\omega_2+\omega_1-\omega_0)\mathcal{E}_3(\omega_1-\omega_0)\right], \qquad \text{(A3)}\end{aligned}$$

$$\begin{aligned}R_{2q}(T_3,T_2,T_1) = \iiint & \frac{d\omega_1 d\omega_2 d\omega_3}{8\pi^3} S^{(3)}(\omega_3,\omega_2,\omega_1)\mathcal{E}_4^*(\omega_3-\omega_0)\\ & \times e^{-i\omega_3 T_3}e^{-i\omega_2 T_2 - i\omega_1 T_1}\mathcal{E}_3^*(-\omega_3+\omega_2-\omega_0)\\ & \times \mathcal{E}_2(\omega_2-\omega_1-\omega_0)\mathcal{E}_1(\omega_1-\omega_0)\\ & + e^{-i\omega_2 T_2 - i(\omega_2-\omega_1)T_1}\mathcal{E}_3^*(-\omega_3+\omega_2-\omega_0)\\ & \times \mathcal{E}_1(\omega_2-\omega_1-\omega_0)\mathcal{E}_2(\omega_1-\omega_0)\\ & + e^{-i(\omega_3-\omega_2+\omega_1)T_2 - i\omega_1 T_1}\mathcal{E}_2(\omega_3-\omega_2-\omega_0)\\ & \times \mathcal{E}_3^*(-\omega_2+\omega_1-\omega_0)\mathcal{E}_1(\omega_1-\omega_0)\\ & + e^{-(\omega_3-\omega_1)T_2 - i(\omega_2-\omega_1)T_1}\mathcal{E}_2(\omega_3-\omega_2-\omega_0)\\ & \times \mathcal{E}_1(\omega_2-\omega_1-\omega_0)\mathcal{E}_3^*(-\omega_1-\omega_0)\\ & + e^{-i(\omega_3-\omega_2+\omega_1)T_2 - i(\omega_3-\omega_2)T_1}\mathcal{E}_1(\omega_3-\omega_2-\omega_0)\\ & \times \mathcal{E}_3^*(-\omega_2+\omega_1-\omega_0)\mathcal{E}_2(\omega_1-\omega_0)\\ & + e^{-i(\omega_3-\omega_1)T_2 - i(\omega_3-\omega_2)T_1}\mathcal{E}_1(\omega_3-\omega_2-\omega_0)\\ & \times \mathcal{E}_2(\omega_2-\omega_1-\omega_0)\mathcal{E}_3^*(-\omega_1-\omega_0). \qquad \text{(A4)}\end{aligned}$$

Essentially, the expressions are identical, just positions of conjugate fields have interchanged. By ordering all integration variables, we obtained more compact expressions,

$$\begin{aligned}R_{nr}(T_3,T_2,T_1) = \iiint & \frac{dx_1 dx_2 dx_3}{8\pi^3}\mathcal{E}_4^*(x_3)\mathcal{E}_3(x_3-x_2)\\ & \times \mathcal{E}_2^*(-x_2+x_1)\mathcal{E}_1(x_1)\exp\left[-i(x_3+\omega_0)T_3\right.\\ & \left. - ix_2 T_2 - i(x_1+\omega_0)T_1\right]\left[S_{4321}^{(3)}(x_3+\omega_0,x_2,x_1+\omega_0)\right.\\ & + S_{4123}^{(3)}(x_3+\omega_0,x_3-x_1,x_3-x_2+\omega_0)\\ & + S_{4231}^{(3)}(x_3+\omega_0,x_3-x_2+x_1+2\omega_0,x_1+\omega_0)\\ & + S_{4213}^{(3)}(x_3+\omega_0,x_3-x_2+x_1+2\omega_0,x_3-x_2+\omega_0)\\ & + S_{4132}^{(3)}(x_3+\omega_0,x_3-x_1,x_2-x_1-\omega_0)\\ & \left. + S_{4312}^{(3)}(x_3+\omega_0,x_2,x_2-x_1-\omega_0)\right], \qquad \text{(A5)}\end{aligned}$$

$$\begin{aligned}R_{III}(T_3T_2T_1) = \iiint & \frac{dx_1 dx_2 dx_3}{8\pi^3}\mathcal{E}_4^*(x_3)\mathcal{E}_3^*(-x_3+x_2)\\ & \times \mathcal{E}_2(x_2-x_1)\mathcal{E}_1(x_1)\exp\left[-i(x_3+\omega_0)T_3\right.\\ & \left. - i(x_2+2\omega_0)T_2 - i(x_1+\omega_0)T_1\right]\\ & \times \left[S_{4321}^{(3)}(x_3+\omega_0,x_2+2\omega_0,x_1+\omega_0)\right.\\ & + S_{4312}^{(3)}(x_3+\omega_0,x_2+2\omega_0,x_2-x_1+\omega_0)\\ & + S_{4231}^{(3)}(x_3+\omega_0,x_3-x_2+x_1,x_1+\omega_0)\\ & + S_{4132}^{(3)}(x_3+\omega_0,x_3-x_1,x_2-x_1+\omega_0)\\ & + S_{4213}^{(3)}(x_3+\omega_0,x_3-x_2+x_1,x_3-x_2-\omega_0)\\ & \left. + S_{4123}^{(3)}(x_3+\omega_0,x_3-x_1,x_3-x_2-\omega_0)\right]. \qquad \text{(A6)}\end{aligned}$$

Note that for the completely off-resonant case corresponding to Kerr-nonlinear material, the rephasing and non-rephasing signals will yield very similar 2D spectra, with just the direction of elongation reversed for pure Gaussian pulse without chirp.

APPENDIX B: FOURIER TRANSFORM OF AN OPTICAL PULSE

Consider a realistic pulse with carrier frequency ω_0 and amplitude profile $\mathcal{E}(t)$, centered at time τ. The optical field of the pulse is then

$$E(t) = \mathcal{E}_t(t-\tau)e^{ikr - i\omega_0(t-\tau)} + c.c. \qquad \text{(B1)}$$

Here, *c.c.* denotes the complex conjugate. Let us characterize the envelope function via its spectral function $\mathcal{E}(\omega)$,

$$\mathcal{E}_t(t) = \int_{-\infty}^{\infty}\frac{d\omega}{2\pi}\mathcal{E}(\omega)e^{-i\omega t}. \qquad \text{(B2)}$$

The resulting Fourier transformed full field can be written as

$$\tilde{E}(\omega) = e^{ikr + i\omega\tau}\mathcal{E}(\omega-\omega_0) + e^{-ikr + i\omega\tau}\mathcal{E}^*(-\omega-\omega_0). \qquad \text{(B3)}$$

Notice that if the time function $\mathcal{E}_t(t)$ is real, we have $\mathcal{E}(\omega) = \mathcal{E}^*(-\omega)$.

This approach allows specifying the simple Gaussian pulses, where $\mathcal{E}(\omega) = \exp(-\omega^2/\sigma^2)$, where spectral pulse width is σ. However, the pure Gaussian pulse is an idealization. Usually, some phase shift is involved during the pulse, causing chirp. The chirped Gaussian pulses, where the frequency changes with pulse time, can be written as

$$E(t) = \exp(-t^2\sigma^2)\exp(i(\omega_0 + rt)t) + c.c. \qquad \text{(B4)}$$

Here, r is the chirp parameter. The phase shift is usually small within the pulse, so $r < \sigma^2$. The Fourier transform of the pulse yields the complex-value envelope function, while still being Gaussian,

$$\mathcal{E}(\omega) = \exp\left(-\frac{\omega^2}{\sigma^2(1-i\xi)}\right), \tag{B5}$$

where we denote $r/\sigma^2 = \xi$ as a dimensionless chirp parameter. Now, we find the complex-value spectral broadening parameter $g = \sigma^2(1 - i\xi)$. Using this notation, the frequency changes linearly within the pulse envelope as $\omega(t) = \omega_0 + \xi\sigma^2 t$. Notice that in this case, the time domain envelope function is not a real-value function, hence $\mathcal{E}(\omega) \neq \mathcal{E}^*(-\omega)$.

APPENDIX C: MULTIDIMENSIONAL QUADRATIC FORMS

A multidimensional Gaussian integral with real coefficients a_{ij},

$$G_{a,b}^{(N)} = \int d^N x \ \exp\left(\sum_{ij}^{i\geq j} a_{ij}x_i x_j + \sum_j b_j x_j\right) \tag{C1}$$

can be calculated by factorizing the exponential. Note that a quadratic form in the exponential can be written in matrix representation,

$$\sum_{ij}^{i\geq j} a_{ij}x_i x_j + \sum_j b_j x_j = (\boldsymbol{x}-\boldsymbol{c})^T \hat{M}(\boldsymbol{x}-\boldsymbol{c}) - \boldsymbol{c}^T\hat{M}\boldsymbol{c}. \tag{C2}$$

Here, $M_{ii} = a_{ii}$ and $M_{ij} = \frac{1}{2}a_{ij}$ for $i \neq j$, and $\boldsymbol{c}$ is the vector of constants, which satisfies $\hat{M}\boldsymbol{c} = \boldsymbol{b}/2$. Hence, $\boldsymbol{c}$ becomes available by solving the linear system of equations. As matrix $\hat{M}$ is symmetric, it can be diagonalized using unitary transformation,

$$\hat{M} = \hat{U}\hat{D}\hat{U}^T, \tag{C3}$$

where D is the diagonal matrix with eigenvalues of matrix $\hat{M}$, while $\hat{U}$ contains all eigenvectors in columns,

$$\hat{M}\hat{U} = \hat{U}D. \tag{C4}$$

Then, we can denote $\hat{U}^T(\boldsymbol{x}-\boldsymbol{c}) = \boldsymbol{y}$ and the integration with respect to x can be changed into y. In addition, assuming that eigenvectors are normalized, we have $d^N x = d^N y$. Then, for the aforementioned integral, we can write

$$\begin{aligned} G_{a,b}^{(N)} &= \exp\left(-\boldsymbol{c}^T\hat{M}\boldsymbol{c}\right)\prod_j^N \int dy_j \ \exp\left(D_{jj}y_j^2\right) \\ &= \pi^{N/2}\frac{\exp\left(-\boldsymbol{c}^T\hat{M}\boldsymbol{c}\right)}{\sqrt{\prod_j^N |D_{jj}|}}. \end{aligned} \tag{C5}$$

Notice that for proper convergence of the integral, all eigenvalues D_{jj} must be negative.

The same expression can be applied for complex coefficients $\boldsymbol{b}$ only if $\hat{M}$ has reals on the off-diagonal part (hence, $\hat{M}$ is symmetric and diagonalizable with the single set of eigenvectors). This also applies for the Hermitian $\hat{M}$ matrix. If the matrix is not Hermitian, then the single set of left and right eigenvectors does not exist and the factorization becomes non-symmetric, makes evaluating the Gaussian integral more complicated.

This analysis allows calculating integrals of Eq. (15). First, the characteristic matrix of the quadratic form in the exponent is

$$\hat{M} = \frac{1}{\sigma^2}\begin{pmatrix} -2 & 1 & 0 \\ 1 & -2 & 1 \\ 0 & 1 & -2 \end{pmatrix}, \tag{C6}$$

and the corresponding vector $\boldsymbol{b} = -i(T_1, T_2, T_3)^T$. The eigenvalue equation allows writing the shift vector $\boldsymbol{c}$ and eigenvalue matrix,

$$\boldsymbol{c} = \frac{i\sigma^2}{8}\begin{pmatrix} 3T_1 + 2T_2 + T_3 \\ 2(T_1 + 2T_2 + T_3) \\ T_1 + 2T_2 + 3T_3 \end{pmatrix}, \tag{C7}$$

$$\hat{D} = -\frac{1}{\sigma^2}\begin{pmatrix} 2 & 0 & 0 \\ 0 & 2+\sqrt{2} & 0 \\ 0 & 0 & 2-\sqrt{2} \end{pmatrix}, \tag{C8}$$

leading to integral value, which is in Eq. (17).

APPENDIX D: PARTIAL INTEGRATION OF THE RESPONSE INTEGRAL

Start with the expression given in Eq. (11). Substituting response function expression Eq. (21) yields three terms,

$$\begin{aligned} R_I(T_3,T_2,T_1) = S_0^{(3)} i\gamma e^{i\omega_0(T_1-T_3)} &\iiint_{-\infty}^{\infty} \frac{dx_1 dx_2 dx_3}{4\pi^3} \\ &\times g(x_3,x_2,x_1)\exp\left(-ix_3T_3 - ix_2T_2 - ix_1T_1\right) \\ &\times \left[\frac{x_2+i\gamma}{(x_2+i\gamma)^2-\nu^2} + \frac{x_3-x_2+x_1+i\gamma}{(x_3-x_2+x_1+i\gamma)^2-\nu^2}\right. \\ &\left. + \frac{x_3-x_1+2\omega_0+i\gamma}{(x_3-x_1+2\omega_0+i\gamma)^2-\nu^2}\right]. \end{aligned} \tag{D1}$$

Here, we have a complex-value Gaussian kernel,

$$g(x_3,x_2,x_1) = \exp\left(-\frac{x_3^2}{g^*} - \frac{(x_3-x_2)^2}{g} - \frac{(x_2-x_1)^2}{g} - \frac{x_1^2}{g^*}\right), \tag{D2}$$

where g is defined as a pulse parameter in Appendix B. Next, in order to separate one integral over the response function, the change of variables is done: in the second integral, $x_3 - x_2 + x_1 = x_2'$ and $x_3 - x_2 = x_1'$, and in the third integral, $x_3 - x_1 = x_2'$ and $x_3 - x_2 \to x_1'$, which yields Gaussian integrals with respect to new variables x_1 and x_3,

$$\begin{aligned} R_I(T_3,T_2,T_1) = \frac{S_0^{(3)}}{4\pi^3} i\gamma e^{i\omega_0(T_1-T_3)} &\int_{-\infty}^{\infty} dx \iint_{-\infty}^{\infty} dx_1 dx_3 \\ &\times \left[\frac{(x+i\gamma)e^{-ixT_2}}{(x+i\gamma)^2-\nu^2} g(x_3,x,x_1)e^{-ix_3T_3-ix_1T_1}\right. \\ &\left. + \frac{(x+i\gamma)e^{-ixT_1}}{(x+i\gamma)^2-\nu^2} g(x_3,x,x-x_1)\right. \end{aligned}$$

$$\times e^{-ix_3(T_3+T_2)+ix_1(T_2+T_1)} + \frac{(x+2\omega_0+i\gamma)e^{ixT_1}}{(x+2\omega_0+i\gamma)^2-\nu^2} \times g(x_3, x_3+x_1-x, x_3-x)e^{-ix_3(T_3+T_2+T_1)+ix_1T_2}\Bigg]. \tag{D3}$$

The double integration over x_1 and x_3 is independent and can be done analytically. Using dimensionless parameters ($\tilde{\gamma} = \gamma/\sigma$, $\tilde{\omega}_0 = \omega_0/\sigma$, $\tilde{\nu} = \nu/\sigma$, and $\tilde{T}_i = \sigma T_i$), this yields

$$R_{rp}(T_3, T_2, T_1) = \frac{i\gamma\sigma^2 e^{-i\tilde{\omega}_0(\tilde{T}_3-\tilde{T}_1)}}{8\pi^2}\int_{-\infty}^{\infty} dx\, \exp\left(-2x^2\right) \times \Bigg[\frac{(x+i\tilde{\gamma})e^{-ix\tilde{T}_2}}{(x+i\tilde{\gamma})^2-\tilde{\nu}^2}\exp\left(f(x,\tilde{T}_1)+f(x,\tilde{T}_3) - 2i\xi x^2\right) + \frac{(x+i\tilde{\gamma})e^{-ix\tilde{T}_1}}{(x+i\tilde{\gamma})^2-\tilde{\nu}^2}\exp\left(f^*(x,\tilde{T}_2+\tilde{T}_1) + f(x,\tilde{T}_3+\tilde{T}_2)\right) + \frac{(x+2\tilde{\omega}_0+i\tilde{\gamma})e^{ix\tilde{T}_1}}{(x+2\tilde{\omega}_0+i\tilde{\gamma})^2-\tilde{\nu}^2} \times e^{(1-i\xi)f(x,-\tilde{T}_2)+(1+i\xi)f^*(x,-\tilde{T}_3-\tilde{T}_2-\tilde{T}_1)}\Bigg]. \tag{D4}$$

Here, the function $f(x,y)$ was defined in Eq. (19). It can be noticed that since $\omega_0 \gg \nu \gg \gamma$, $\sigma \sim \nu$, and the third term in the above-mentioned expression is proportional to $\tilde{\omega}_0^{-1}$, while the other two terms ~1. As a result, it can be dropped, which yields Eq. (22).

REFERENCES

[1] T. Brixner, I. V. Stiopkin, and G. R. Fleming, Opt. Lett. **29**, 884 (2004).
[2] T. Hornung, J. C. Vaughan, T. Feurer, and K. A. Nelson, Opt. Lett. **29**, 2052 (2004).
[3] G. S. Engel, T. R. Calhoun, E. L. Read, T.-K. Ahn, T. Mančal, Y.-C. Cheng, R. E. Blankenship, and G. R. Fleming, Nature **446**, 782 (2007).
[4] T. Brixner, J. Stenger, H. M. Vaswani, M. Cho, R. E. Blankenship, and G. R. Fleming, Nature **434**, 625 (2005).
[5] E. Collini, C. Y. Wong, K. E. Wilk, P. M. G. Curmi, P. Brumer, and G. D. Scholes, Nature **463**, 644 (2010).
[6] J. Dostál, J. Pšenčík, and D. Zigmantas, Nat. Chem. **8**, 705 (2016).
[7] H. L. Nguyen, T. N. Do, K. Zhong, P. Akhtar, T. L. C. Jansen, J. Knoester, S. Caffarri, P. Lambrev, and H.-S. Tan, Sci. Adv. **10**, eadh0911 (2024).
[8] E. Fresch, E. Meneghin, A. Agostini, H. Paulsen, D. Carbonera, and E. Collini, J. Phys. Chem. Lett. **11**, 1059 (2020).
[9] A. M. Brańczyk, D. B. Turner, and G. D. Scholes, Ann. Phys. **526**, 31 (2014).
[10] A. D. Sio, F. Troiani, M. Maiuri, J. Réhault, E. Sommer, J. Lim, S. F. Huelga, M. B. Plenio, C. A. Rozzi, G. Cerullo, E. Molinari, and C. Lienau, Nat. Commun. **7**, 13742 (2016).
[11] Y. Song, R. Sechrist, H. H. Nguyen, W. Johnson, D. Abramavicius, K. E. Redding, and J. P. Ogilvie, Nat. Commun. **12**, 2801 (2021).
[12] H. H. Nguyen, Y. Song, E. L. Maret, Y. Silori, R. Willow, C. F. Yocum, and J. P. Ogilvie, Sci. Adv. **9**, eade7190 (2023).
[13] G. Marcolin and E. Collini, J. Phys. Chem. Lett. **12**, 4833 (2021).
[14] F. D. Fuller, J. Pan, A. Gelzinis, V. Butkus, S. S. Senlik, D. E. Wilcox, C. F. Yocum, L. Valkunas, D. Abramavicius, and J. P. Ogilvie, Nat. Chem. **6**, 706 (2014).
[15] E. Romero, R. Augulis, V. I. Novoderezhkin, M. Ferretti, J. Thieme, D. Zigmantas, and R. van Grondelle, Nat. Phys. **10**, 676 (2014).
[16] J. Lim, D. Paleček, F. Caycedo-Soler, C. N. Lincoln, J. Prior, H. von Berlepsch, S. F. Huelga, M. B. Plenio, D. Zigmantas, and J. Hauer, Nat. Commun. **6**, 7755 (2015).
[17] Y. Song, A. Schubert, E. Maret, R. K. Burdick, B. D. Dunietz, E. Geva, and J. P. Ogilvie, Chem. Sci. **10**, 8143 (2019).
[18] A. Niedringhaus, V. R. Policht, R. Sechrist, A. Konar, P. D. Laible, D. F. Bocian, D. Holten, C. Kirmaier, and J. P. Ogilvie, Proc. Natl. Acad. Sci. U. S. A. **115**, 3563 (2018).
[19] E. Bukartė, A. Haufe, D. Paleček, C. Büchel, and D. Zigmantas, Chem. Phys. **530**, 110643 (2020).
[20] V. Butkus, J. Alster, E. Bašinskaitė, R. Augulis, P. Neuhaus, L. Valkunas, H. L. Anderson, D. Abramavicius, and D. Zigmantas, J. Phys. Chem. Lett. **8**, 2344 (2017).
[21] E. Thyrhaug, R. Tempelaar, M. J. P. Alcocer, K. Žídek, D. Bína, J. Knoester, T. L. C. Jansen, and D. Zigmantas, Nat. Chem. **10**, 780 (2018).
[22] D. Abramavicius, D. V. Voronine, and S. Mukamel, Biophys. J. **94**, 3613 (2008).
[23] B. Huber, S. Pres, E. Wittmann, L. Dietrich, J. Lüttig, D. Fersch, E. Krauss, D. Friedrich, J. Kern, V. Lisinetskii, M. Hensen, B. Hecht, R. Bratschitsch, E. Riedle, and T. Brixner, Rev. Sci. Instrum. **90**, 113103 (2019).
[24] S. Goetz, D. Li, V. Kolb, J. Pflaum, and T. Brixner, Opt. Express **26**, 3915 (2018).
[25] V. Tiwari, Y. A. Matutes, A. T. Gardiner, T. L. C. Jansen, R. J. Cogdell, and J. P. Ogilvie, Nat. Commun. **9**, 4219 (2018).
[26] A. Javed, J. Lüttig, K. Charvátová, S. E. Sanders, R. Willow, M. Zhang, A. T. Gardiner, P. Malý, and J. P. Ogilvie, J. Phys. Chem. Lett. **15**, 12376 (2024).
[27] P. Malý, J. Lüttig, P. A. Rose, A. Turkin, C. Lambert, J. J. Krich, and T. Brixner, Nature **616**, 280 (2023).
[28] V. Bubilaitis and D. Abramavicius, J. Chem. Phys. **161**, 104106 (2024).
[29] B. Kriete, J. Lüttig, T. Kunsel, P. Malý, T. L. C. Jansen, J. Knoester, T. Brixner, and M. S. Pshenichnikov, Nat. Commun. **10**, 4615 (2019).
[30] J. S. J. Wehner, J. Dostál, T. Brixner, and V. Engel, J. Chem. Phys. **150**, 104304 (2019).
[31] H. H. Nguyen, A. D. Loukianov, J. P. Ogilvie, and D. Abramavicius, J. Chem. Phys. **153**, 144203 (2020).
[32] J. Yang, M. F. Gelin, L. Chen, F. Šanda, E. Thyrhaug, and J. Hauer, J. Chem. Phys. **159**, 074201 (2023).
[33] E. Collini, J. Phys. Chem. C **125**, 13096 (2021).
[34] E. Fresch, F. V. A. Camargo, Q. Shen, C. C. Bellora, T. Pullerits, G. S. Engel, G. Cerullo, and E. Collini, Nat. Rev. Methods Primers **3**, 84 (2023).
[35] Y. Song, S. N. Clafton, R. D. Pensack, T. W. Kee, and G. D. Scholes, Nat. Commun. **5**, 4933 (2014).
[36] D. Zigmantas, T. Polívka, P. Persson, and V. Sundström, Chem. Phys. Rev. **3**, 041303 (2022).
[37] A. H. Proppe, Y. C. Li, A. Aspuru-Guzik, C. P. Berlinguette, C. J. Chang, R. Cogdell, A. G. Doyle, J. Flick, N. M. Gabor, R. van Grondelle, S. Hammes-Schiffer, S. A. Jaffer, S. O. Kelley, M. Leclerc, K. Leo, T. E. Mallouk, P. Narang, G. S. Schlau-Cohen, G. D. Scholes, A. Vojvodic, V. W.-W. Yam, J. Y. Yang, and E. H. Sargent, Nat. Rev. Mater. **5**, 828 (2020).
[38] S. M. Hart, W. J. Chen, J. L. Banal, W. P. Bricker, A. Dodin, L. Markova, Y. Vyborna, A. P. Willard, R. Häner, M. Bathe, and G. S. Schlau-Cohen, Chem **7**, 752 (2021).
[39] M. Son, A. Pinnola, S. C. Gordon, R. Bassi, and G. S. Schlau-Cohen, Nat. Commun. **11**, 1295 (2020).
[40] Y. Song, A. Schubert, X. Liu, S. Bhandari, S. R. Forrest, B. D. Dunietz, E. Geva, and J. P. Ogilvie, J. Phys. Chem. Lett. **11**, 2203 (2020).
[41] C. Gajo, C. J. C. Jordan, and T. A. A. Oliver, J. Phys. Chem. A **129**, 3537 (2025).
[42] S. S. Mukamel, *Principles of Nonlinear Optical Spectroscopy* (Oxford University Press, New York, 1995).
[43] D. Abramavicius, B. Palmieri, D. V. Voronine, F. Šanda, and S. Mukamel, Chem. Rev. **109**, 2350 (2009).
[44] L. Valkunas, D. Abramavicius, and T. Mančal, *Molecular Excitation Dynamics and Relaxation* (Wiley-VCH Verlag GmbH & Co. KGaA, 2013).
[45] A. Gelzinis, R. Augulis, V. Butkus, B. Robert, and L. Valkunas, Biochim. Biophys. Acta, Bioenerg. **1860**, 271 (2019).

[46]D. Paleček, P. Edlund, E. Gustavsson, S. Westenhoff, and D. Zigmantas, J. Chem. Phys. **151**, 024201 (2019).
[47]A. Hedse, A. A. S. Kalaee, A. Wacker, and T. Pullerits, J. Chem. Phys. **158**, 141104 (2023).
[48]E. E. Ostroumov, R. M. Mulvaney, R. J. Cogdell, and G. D. Scholes, Science **340**, 52 (2013).
[49]M. W. Graham, T. R. Calhoun, A. A. Green, M. C. Hersam, and G. R. Fleming, Nano Lett. **12**, 813 (2012).
[50]S. M. Gallagher Faeder and D. M. Jonas, Phys. Rev. A **62**, 033820 (2000).
[51]N. Geoffrey, *Introduction to Nonlinear Optics* (Cambridge University Press, 2011).
[52]A. Taschin, P. Bartolini, R. Eramo, R. Righini, and R. Torre, J. Chem. Phys. **141**, 084507 (2014).
[53]B. M. Auer and J. L. Skinner, J. Chem. Phys. **128**, 224511 (2008).
[54]E. Courtens, M. Foret, B. Hehlen, and R. Vacher, Solid State Commun. **117**, 187 (2001).
[55]A. S. Sardjan, F. P. Westerman, J. P. Ogilvie, and T. L. C. Jansen, J. Phys. Chem. B **124**, 9420 (2020).
[56]D. Abramavicius and S. Mukamel, J. Chem. Phys. **122**, 134305 (2005).
[57]Z. Wang, A. Hedse, E. Amarotti, N. Lenngren, K. Žídek, K. Zheng, D. Zigmantas, and T. Pullerits, J. Chem. Phys. **157**, 014201 (2022).
[58]V. Butkus, D. Zigmantas, D. Abramavicius, and L. Valkunas, Chem. Phys. Lett. **587**, 93 (2013).